The effects of ageing on mouse muscle microstructure: A comparative study of time-dependent diffusion MRI and histological assessment

Short title: Age-related changes in muscle microstructure by dMRI and histology

Paola Porcari[a*], Matt G Hall[b], Chris A Clark[b], Elizabeth Greally[c], Volker Straub[c], and Andrew M Blamire[d]

*Correspondence to: Paola Porcari, Newcastle Magnetic Resonance Centre, Campus for Ageing and Vitality, Newcastle University, Newcastle Upon Tyne, UK. E-mail: paola.porcari@ncl.ac.uk

a *Paola Porcari*

Institute of Genetic Medicine and Centre for In Vivo Imaging, Newcastle University, Newcastle upon Tyne, UK

b *Matt G Hall, Chris A Clark*

Developmental Imaging and Biophysics Section, UCL GOS Institute of Child Health, University College London, London, UK

c *Elizabeth Greally, Volker Straub*

John Walton Muscular Dystrophy Research Centre, Institute of Genetic Medicine, Newcastle University, Newcastle upon Tyne, UK

d *Andrew M Blamire*

Institute of Cellular Medicine and Centre for In Vivo Imaging, Newcastle University, Newcastle upon Tyne, UK

Abstract

The investigation of age-related changes in muscle microstructure between developmental and healthy adult mice may help in understanding the clinical features of early-onset muscle diseases, such as Duchenne muscular dystrophy.

We investigated the evolution of mouse hind-limb muscle microstructure using diffusion imaging of *in vivo* and *in vitro* samples from both actively-growing and mature mice. Mean apparent diffusion coefficients (ADCs) of the gastrocnemius and tibialis anterior muscles were determined as a function of diffusion time (Δ), age (7.5-, 22- and 44-week-old) and diffusion-gradient direction, applied parallel or transverse to the principal axis of the muscle fibres. We investigated a wide range of diffusion times with the goal of probing a range of diffusion lengths characteristic of muscle microstructure. We compared the diffusion time-dependent ADC of hind-limb muscles with histology.

ADC was found to vary as a function of diffusion time in muscles at all stages of maturation. Muscle water diffusivity was higher in younger (7.5-week-old) than in adult mice (22- and 44-week-old mice), whereas no differences were observed between the older ages. *In vitro* data showed the same diffusivity pattern as *in vivo* data. The highlighted differences in diffusion properties between young and mature muscles suggested differences in underlying muscle microstructure, which were confirmed by histological assessment. In particular, while diffusion was more restricted in older muscle, muscle fibre size increased significantly from young to adult age. The extracellular space decreased with age by only ~1%. This suggests that the observed diffusivity differences between young and adult muscles may be due to increased membrane permeability in younger muscle associated with properties of the sarcolemma.

Keywords: time-dependent diffusion MRI, diffusion MRI, Apparent Diffusion Coefficient, Diffusion Weighted Imaging, hind-limb muscles, mouse, maturation, histology

Abbreviations used: *ADC, apparent diffusion coefficient; ANOVA, analysis of variance; δ, gradient-pulse-duration; Δ, gradient-pulses-separation, diffusion time; dMRI, diffusion MRI; DWI, diffusion weighted imaging; EBD, Evans Blue Dye; FFPE, formalin fixed paraffin embedded;* $l = (2D\Delta)^{1/2}$ *diffusion distance; GA, gastrocnemius muscle; Gdiff, diffusion gradient direction*; *H&E, haematoxylin and eosin; myofibres, multinucleated muscle fibre; myonuclei, (myofibre nuclei); PGSTE, pulse gradient stimulated echo; ROI, region of interest; TA, tibialis anterior muscle.*

INTRODUCTION

Skeletal muscle is the most abundant tissue in the human body, comprising 30-40% of the body weight [1], and is the major site of metabolic activity [2]. Its function, which is strictly dependent on muscle cytoarchitecture [3], enables vital actions, i.e. breathing, posture, and locomotion, and affects systemic processes such as homeostasis and the immune response.

Skeletal muscle mass and fibre size vary according to physiological and pathological conditions [4], which influence the pathways regulating the balance between protein synthesis and degradation within muscle fibres [5]. During postnatal development, this equilibrium, which determines cell size, may be affected by the incorporation of myogenic stem cells into the multinucleated myofibres [6]. This allows the addition of myonuclei, each of them with its myonuclear domain defined as the cytoplasmic volume per myonucleus [4]. This process causes enlarged myofibre volume due to an increase in both cross-sectional area and length and is concurrent with increased protein synthesis within myofibres leading to muscle growth or hypertrophy [5]. During this period of hypertrophy, which in mice ends by 12 weeks of age [7, 8], the sarcolemma dynamically and constantly expands, whereas during adult life it maintains almost the same size under normal healthy condition [6]. Investigation of myofibre sizes and sarcolemmal properties in actively growing and mature myofibres in homeostasis could have major implications for understanding the clinical onset of particular genetic muscle diseases, such as Duchenne muscular dystrophy and dysferlinopathies [9-10], where significant changes in size composition occur with disease progression.

Diffusion MRI [11] is known to be sensitive to tissue microstructure [12-13], including at cellular and sub-cellular length scales [14] and has been used to investigate both muscle structure [15-17] and function [18-20]. The contrast mechanism underlying diffusion-weighted images relies on the random microscopic motion of water molecules [13] within the tissue micro-environment during a defined diffusion time (Δ). By increasing Δ, the sensitivity of diffusion MRI to tissue microstructure increases with the degree of interactions between the diffusing water molecules and the existing structural barriers, such as cell membranes, the cytoskeleton and macromolecules,

which together influence the overall water mobility. Muscle tissue is characterised by myofibre sizes ranging from 10 to 80 μm [21] and so long Δ must be used to explore these extended length scales. The dependence of the apparent diffusion coefficient (ADC) on Δ may be then used to characterise restrictions and/or hindrances in the water microenvironment.

Time-dependence in the diffusion coefficient using DWI was first observed by Tanner in diffusion-weighted images of *ex-vivo* frog muscle tissue [22]. This effect was used to estimate myofibre size and sarcolemmal permeability. Since then, other studies have measured the time dependence of diffusivity in skeletal muscle [23-27], other organs [28-30], and in other pathologies [31-32]. More recently, structural parameters, such as fibre size and membrane permeability of human calf muscles, have been quantified in both adult healthy subjects [23, 26] and patients [26] by using a biophysical model [33] applied to time-dependent diffusion measurements. However, these findings have not been validated against an independent microstructural gold-standard provided by histology.

The aim of this study was to apply diffusion imaging to assess the evolution of hind-limb muscle microstructure between healthy mice of three age groups, covering development and adulthood. The time dependence of the ADC was measured both *in vivo* and *in vitro* in hind-limb muscles. Diffusion-weighted images with multiple *b*-values were acquired over a range of Δ and with diffusion gradients applied parallel or transverse to the main axes of the muscle fibres. Imaging data are compared to histological assessments of muscle fibre size, sarcolemmal integrity and estimates of the extracellular space.

2. MATERIALS AND METHODS

2.1 Animals, MRI preparation

Male C57BL/10ScSnOlaHsd mice (Harlan Laboratories, Indianapolis, IN, USA) of three age groups, 7.5 (n = 8, mouse weight = 22 - 28 g), 22 (n = 8; mouse weight = 34 - 42 g) and 44 (n = 4; mouse weight = 36 - 45 g) weeks old were used in this study. Mice were housed and treated in accordance with the Animals (Scientific Procedures) Act 1986, authorised by the Home Office UK and the work was approved by the Ethical Review Committee of Newcastle University.

Before imaging, induction of anaesthesia was performed using 4% isoflurane mixed with 1 l/min of O_2. Anaesthetised mice were laid supine in a custom-built holder positioned and held to ensure minimal motion during MR imaging. Anaesthesia was maintained at 1.5 - 2 % of isoflurane mixed with 0.5 – 1 l/min of O_2 and physiological monitoring was performed using an MR-compatible small animal monitoring and gating system (Model 1025, SA Instruments Inc., Stony Brook, NY, USA). Care was taken to maintain respiration and body temperature at 60 ± 20 bpm and 37 ± 0.5 °C, respectively. Following *in vivo* MRI, mice were euthanised and both hind-limbs dissected and skinned. The right hind-limbs were collected for immediate fixation and *in vitro* MRI measurements whereas the left hind-limbs were processed for histology, immunohistochemistry and muscle fibre size determination. Selected animals were injected with Evans Blue Dye (EBD) prior to euthanasia to reveal any differences in muscle fibre membrane integrity.

2.2 *In vivo* MRI

MRI experiments were performed on a 7T / 21 cm horizontal bore magnet (Magnex Scientific, Oxford, UK) interfaced to a Direct Drive console (Agilent, Palo Alto, CA, USA) equipped with a 12-cm inner diameter (i.d.) actively-shielded gradient set (400 mT/m in 150 µs). Mice were imaged using a 30 mm i.d. quadrature volume transceiver coil (Rapid Biomedical GmbH, Germany). After collecting scout images to confirm positioning, a series of axial T_2-weighted fast spin-echo (FSE) images was acquired with effective echo time (TE_{eff}) = 48 ms, repetition time (TR) = 5000 ms, echo train length = 8, field-of-view (FOV) = 20 × 20 mm^2, acquisition matrix = 256 × 256, in-plane-resolution of 78 µm × 78 µm, 5 slices of 1 mm thickness; 2 averages and scan time of 5 min. First and second order shims were adjusted using an automated 3D gradient shimming routine, resulting in water linewidths of 20-26 Hz for a volume of interest of 3.8 × 3.8 × 4 mm^3, centred in the lower hind-limb. DWI scans were performed with slice orientation perpendicular to the tibial bone, using a pulse-gradient-stimulated-echo (PGSTE) sequence [34] with TE = 22 ms, TR = 4000 ms, bandwidth = 20 KHz; FOV= 20 × 10 mm^2, acquisition matrix = 128 × 64, in-plane resolution of 156 µm × 156 µm and 5 slices of 1 mm thickness, sufficient to cover the whole lower hind-limb. Six Δ values equal to 25, 60, 100, 150, 250 and 350 ms were

selected for the *in vivo* experiment based on *in vitro* observation in a pilot study (Supporting Information, Figure S1), which was carried out in a mouse hind-limb fixed in formalin (4% buffered formalin). For each Δ, DWI data were acquired using three *b*-values (Table 1), gradient duration (δ) of 3 ms and the diffusion gradient applied parallel (slice-selection direction) or transverse (phase-encoding direction) to the main axis of the muscle. The calculated *b*-values includes the contribution of imaging and crusher gradients, which lead to non-zero b_0 values for the un-weighted diffusion images, as reported in Table 1. Scans at Δ = 25 and 60 ms used 1 average resulting in 12 min acquisition time, whereas 2 averages were used for all other Δ resulting in 25 min of scan time each. Total acquisition time was 124 min. In 7.5-week-old mice scan time was reduced to 100 min by omitting the intermediate Δ value of 150 ms.

As T_1 relaxation of the diffusion-weighted signal occurs during the Δ period, muscle water T_1 was measured to assess possible contribution of T_1 changes to ADC data. Measurements were carried-out on three mice per age group using an inversion-recovery FSE sequence with TE_{eff} = 23.43 ms, TR = 4000 ms, echo train length = 8, inversion times (TI) = 50, 83, 140, 230, 390, 650, 1080, 1800 ms, 2 averages and scan time of 8 min 40 sec. Scan geometry was the same as for the DWI scans.

2.3 Data analysis

Regions-of-interest (ROIs) were drawn on the diffusion-weighted images in the gastrocnemius (GA) and tibialis anterior (TA) muscles (Figure 1) using a circular area of 0.026 mm^2 for all the acquired slices, carefully avoiding bone and chemical shift fat artefacts. In these wild type animals, muscle fat content is very low. For each mouse, apparent diffusion coefficient (ADC) of muscles were calculated per diffusion time (Δ) and diffusion gradient direction by fitting the mean signal (S) intensities from ROIs drawn on each slice of the diffusion-weighted images as a function of *b*-value:

$$S(b) = S(0)\cdot\exp(-b\cdot ADC) \quad (1)$$

A justification for using this mono-exponential model is explained in the supplementary data provided in Figure S2. Fitting was performed using a custom Matlab script (Matlab R2012a, The MathWorks). In addition, ADC maps of lower hind-limb were also computed for visual inspection and presentation by fitting, voxel by voxel, the signal intensity (S) of the diffusion-weighted images as function of *b*-values using the scanner software (VnmrJ 4.2, Varian, Palo Alto, USA) (1) (Figure 1).

The signal-to-noise-ratio (SNR) of each muscle was determined for each Δ on the b_0 image as the mean signal intensity of a ROI drawn in the muscle <S> divided by the standard deviation σ of a large ROI in the background noise (*N*) that was visually devoid of artefacts

$$SNR = \langle S \rangle / \sigma(N) \quad (2)$$

The T_1 relaxation times of both muscles was measured and quantified using the same ROIs as for the DWI analysis. T_1 was determined per slice by fitting the mean ROI signal intensities as function of TI

$$S(TI) = S(0)\cdot(1-2\cdot\exp(-TI/T_1)) \quad (3)$$

Mean T_1 in the GA and TA muscles was determined by considering each slice in all the selected animals per age group.

2.4 *In vitro* MRI

Following *in vivo* measurements, anaesthetised mice were euthanised and hind-limbs de-skinned, and removed. Excised right limbs were immersed in an Eppendorf conical tube of 50 mL filled with a solution of 10% neutral buffered formalin (NBF, Sigma-Aldrich, St. Louis, MO, USA). After 24 hours of complete fixation, the hind-limb was removed from the formalin solution. The sample was inserted within a 20 mL sterile Universal tube in order to avoid any movements, then positioned in the scanner and measured using the same MRI protocol as for the *in vivo* measurements. During MRI acquisition, the temperature was 19.0 ± 0.5 °C and it was monitored as for *in vivo* measurements. Data analysis was performed in the same way as for the *in vivo* data.

2.5 Histology and immunohistochemistry for Feret's diameter measurements

Tissue analysis was performed using the standard formalin-fixed paraffin-embedded (FFPE) procedure for histology and the frozen-section procedures for immunohistochemistry. Mice of each age group were randomly divided into two subgroups, which were assigned for haematoxylin and eosin (H&E) staining or laminin immunofluorescence staining, respectively. To evaluate muscle fibre size distributions in each muscle and changes with maturation and age, the Feret's diameter of muscle fibres [21] was measured (ImageJ; https://imagej.nih.gov/ij) analysing all fields imaged in both muscles from specimens stained with H&E (Supporting Information, Section S3.1) or immunofluorescence (Supporting Information, Section S3.2).

2.6 Evans Blue dye uptake

To assess muscle membrane integrity, EBD (Sigma-Aldrich, St. Louis, MO, USA) was used. Mice selected for immunofluorescence staining were injected intraperitoneally with 50 µl per 10 g of body weight of a sterile EBD solution (10 mg EBD/1ml PBS) 24 hours prior to euthanasia. To quantify EBD uptake, samples of frozen muscles were examined. Details are provided in Section S3.3 (Supporting Information). The percentage of EBD positive area, *P*, was determined for each muscle per mouse by considering the contribution from all the selected fields (N = 10) per mouse as given by:

$$P = 100 \times \left(\sum_{j=1}^{N} E_j \Big/ \sum_{j=1}^{N} A_j\right) \tag{4}$$

where the term E_j is the EBD positive area measured in the j-th image, and A_j is the total area of that image. For each selected field, the EBD positive area was measured using the wand tool (ImageJ) which traces objects of uniform colour throughout the image field of view. In this case the red staining is representative of EBD uptake. Before being processed for EBD quantification, the same threshold was applied to all the selected images. Threshold was defined on the images from the TA muscle aged 44 weeks and applied to all other age groups.

2.7 Statistical analysis

Statistical analysis was performed using SPSS (IBM Corp. Released 2013. IBM SPSS Statistics for Windows, Version 22.0. Armonk, NY: IBM Corp. Armonk, NY).

Values are reported as mean ± standard error (s.e.m) for both *in vivo* and *in vitro* data. Statistically significant differences between the mean ADC values across age groups, calculated per Δ, diffusion gradient direction and muscle, were determined with one-way ANOVA followed by Tukey post-hoc test. Differences in mean ADC values between GA and TA muscles, per age group were considered with a two-tailed paired, Student's *t* test. The same statistical analysis was applied to the mean values of T_1 relaxation time.

Statistically significant differences between muscle fibre size distributions among age groups, per muscle, as well as among muscles per age group, were determined using a two sample Kolmogorov-Smirnov (K-S) test.

In all statistical analysis $p < 0.05$ was taken as significant.

3. RESULTS

3.1 *In vivo* MRI findings

In vivo mean muscle ADC values in mice of each of the three age groups (7.5-, 22- and 44-week-old) for each Δ and diffusion gradient direction are shown in Table 2 and plotted in Figure 2A for the GA and Figure 2B for the TA. Muscle water ADC was observed to decrease with increasing Δ, indicating greater restriction at the longer diffusion times. Mean muscle ADC values were higher for all ages when measured parallel to fibres (dashed lines) rather than transverse to them (solid lines) in keeping with expected muscle fibre anisotropy. Overall, the range of SNR in both hind-limb muscles varied from (34 ± 2) at Δ = 25 ms to (21 ± 1) at Δ = 350 ms.

3.1.1 *In vivo* MRI findings – Age-related changes

An age-dependent decrease in muscle water diffusivity was observed between 7.5 and 22 weeks for each Δ and diffusion gradient direction (Table 2, Figure 2), whereas no differences were found between mice aged 22 and 44 weeks. Statistically significant differences between hindlimb muscle mean ADC in young (7.5-week-old) and mature (22- week-old or 44-week-old) mice were found for long Δ (> 250ms) in the GA muscle ($p < 0.01$, Table 2) when the diffusion gradient was

parallel to fibres, and in the TA muscle ($p < 0.01$, Table 2) in both the parallel and transverse cases.

3.1.2 *In vivo* MRI finding – muscle differences

Figure 3 shows the comparison between ADC values in TA and GA muscles for each age group: 7.5 (Figure 3A), 22 (Figure 3B) and 44 weeks (Figure 3C). Compared with the GA muscle, water diffusivity in the TA muscles was higher when the diffusion gradient was parallel to fibres and lower when the diffusion gradient was transverse to fibres (Table 2, Figure 3). Values were significantly different for long Δ in mice aged 22 weeks for both gradient directions (Table 2).

3.1.3 *In vivo* MRI finding – T_1 results

In vivo mean T_1 relaxation times of both GA and TA muscles from mice of each age group (7.5-, 22- and 44-week-old) are summarised in Table 3. No statistically significant differences were found either as a function of mouse age in either muscle, indicating that the ADC characteristics were not significantly influenced by alterations in tissue relaxation characteristics.

3.2 *In vitro* MRI findings

In vitro mean ADC values for muscles dissected from mice in each age group (7.5-, 22- and 44-week-old) are shown in Table 4 and Figures 4 and 5. *In vitro* data showed the same pattern of diffusivity as the *in vivo* data (Figures 2 and 3) although with lower absolute values attributed to changes in microstructure associated with the fixation process.

3.2.1 *In vitro* MRI findings – Age-related changes

As with the *in vivo* data, a significant decrease in ADC values was found with increasing mouse age from 7.5 to 22 weeks ($p > 0.01$, Table 4) with no further statistically significant differences found between 22 and 44 weeks. ADC values were significantly different for long Δ in the GA muscle for both diffusion gradient directions, whereas the TA muscle showed significantly different ADC values only when the diffusion gradient was parallel to fibres (Table 4).

3.3 Histology, immunohistochemistry and Feret's diameter results

Muscle fibre size distributions of both GA and TA muscles were quantified per age group by considering Feret's diameter data measured using the H&E (Figure 6) and laminin staining (Supporting Information, Figure S3) procedures.

Figure 6 shows representative areas of H&E stained cross-sections of the GA muscle dissected from mice of each age group (Figures 6A-C, respectively) and frequency histograms of GA and TA muscle fibre size distributions per age group (Figures 6D-H). For both the GA and TA muscles, fibre size shifted towards larger diameters with increasing age (Figure 6D, E; Supporting Information Table S1). Muscle fibre sizes of both TA and GA muscles increased significantly ($p < 0.001$) between 7.5 and 22 weeks of age with no significant changes observed between 22-week-old and 44-week-old mice. Differences between GA and TA muscle fibre size distributions for each age group were statistically significant (Figures 6F-H) ($p<0.01$).

Feret's diameter data measured on laminin stained sections demonstrated the same trend of increasing muscle fibre size between 7 and 22 weeks (Supporting Information, Figure S3, Table S2).

3.4 Evans Blue Dye results

Percentages of Evans Blue Dye (EBD) positive uptake from the GA and TA muscles per age group are summarised in Table 5 and illustrated in Figure 7. EBD uptake was essentially confined to the small interstitial space between the muscle fibres of the GA muscle. Data showed a decrease of EBD positive area with increasing mouse age for both GA and TA muscles, but it is noted that all values are small and indicate that muscle fibres themselves are essentially impermeable to EBD. Comparison between GA and TA muscles showed higher positive EBD area in the GA muscle for each age group (Table 5, Figure 7).

4. Discussion

We have presented a comparative study of diffusion MRI and histology for the investigation of age-related changes in muscle microstructures of hind-limb in healthy mice. Different diffusion properties were found in each muscle with increasing mouse age (Figure 2-3) by exploring images acquired at selected Δ with the diffusion gradient parallel or transverse to muscle fibres.

Stimulated echo (STE) based DWI sequences offer advantages over conventional spin-echo (SE) sequences [35] as they allow the investigation of diffusion properties over a much broader range of Δ than is possible with a SE acquisition [34]. This is particularly important in muscle tissue [22-23, 26]where long Δ are required to explore the restricted diffusion regime within the large cross-sectional dimensions of the muscle fibres (range 10 - 80 μm) [20]. With increasing Δ, water diffusion tends to a finite non-zero value. This is likely due to the presence of water exchange between intra- and extra-cellular spaces because of the finite water permeability of cell membranes [36-37]. On the other hand, at short Δ which correspond to diffusion lengths much smaller than the typical separation between barriers, only a very small proportion of spins have interacted with restricting structure and the overall diffusion behaviour is less restricted. Therefore, Δ plays an important role in probing muscle structure.

Our findings show a Δ dependence of the mean ADC values determined for each muscle, age group and diffusion-gradient direction in good agreement with previous *in vivo* muscle studies [23, 26]. In particular, ADC was lower and showed a more pronounced reduction with increasing Δ when the diffusion-gradient was applied transverse to fibres rather than parallel to them. This is consistent with diffusive behaviour in the highly ordered muscle structure consisting of parallel fibres and sub-cellular components (myo-fibrils and myosin chains) all oriented along the primary muscle axis.

Our measurements show that water diffusivity decreases in muscle with increasing mouse age from early development (7.5-week-old) to the mature adult age (22- and/or 44-week-old). In particular, when diffusivity is measured parallel to the myofibres the ADC time-dependent curve is shifted downwards between the young and mature mice, suggesting an overall absolute reduction in diffusivity within the tissue environment, independent of the muscle fibre size. When water diffusivity is measured transverse to myofibres the ADC time-dependent curves are again shifted downwards between young and mature mice but also show differences in curvature, which were particularly evident in the GA both *in vivo* and *in vitro*. Change in curvature is indicative of alterations in the restriction due to overall permeability of the internal structure between young

and mature muscles. It is possible therefore that the higher ADC values observed across the studied diffusion time range in young muscle is due to greater fibre permeability in the 7.5-week-old animals compared to 22- and 44-week-old animals and that this effect dominates over ADC differences arising from fibre size [37].

Time dependent diffusivity is indicative of restriction in a non-homogeneous environment. Under these circumstances, the spin displacement probability distribution will deviate from a Gaussian and violate the validity of the approximation of mono-exponential decay (1). Non-Gaussian diffusion is frequently observed in studies of brain, for example, where it is an important component of microstructural imaging approaches [37, 38]. Although our data in muscle did show time dependent behaviour, the diffusion based signal attenuation at each specific diffusion time were all well fit using a mono-exponential function with accuracy of $r^2 \leq 0.99$ across all diffusion gradient strengths. To further understand the diffusion behaviour within the investigated muscles, we obtained measurements over a range of *b*-values as a function of gradient strength (17 values ranging from 78-2500s/mm^2), and found only a weak non-monoexponential behaviour at *b*-values less than 500 s/mm^2 (Supporting Information, Figure S2). The observation that there is no strong non-Gaussian behaviour, even in the highly ordered and multi-compartmental environment of the muscle is consistent with a system with highly permeable barriers. Future studies are required to corroborate this conclusion through attempts at direct quantification of membrane permeability by other means.

Histological analysis showed that mean muscle fibre size increased with age from the young (7.5-week-old) to the mature age (22- or 44-week-old), in line with previous investigations (39). This scenario should lead to lower restriction and increased diffusivity if the main contribution to water diffusivity was driven by interactions between the intra-cellular water and the muscle fibre membrane. However, the observation of higher ADC in younger mice strongly suggests that change in fibre diameter distribution is not the dominant effect on the signal. A recent simulation study suggested that although fibre size change does affect the signal, the effect is not as strong as changes such as permeability [37]. Although, recent studies in human calf muscle in healthy

adult volunteers have estimated myofibre size using an approach which considers diffusion tensors fitted at variable diffusion time [23, 26], our results indicate that care must be taken to avoid bias when extrapolating methods across different age groups.

An additional potential contributory factor may arise from differences in extracellular space between young and old muscle as shown by staining with EBD. The latter is an azo-dye molecule that is normally used in pathology to evaluate membrane's integrity [40]. Due to its hydrophilic nature, it does not cross healthy cell membrane and accumulates in the interstitial/extracellular space. Our measurements showed a decrease in the percentage of EBD uptake in both GA and TA muscles with increasing age which, in turn, suggests a decrease of the extracellular volume (Figure 7). However, the measured percentages in the histologically sampled regions are small (only 2.5% and 1.5% in the GA muscle of young and mature mice, respectively), so the effect of changes in extra-cellular space on ADC is likely to be negligible. A further factor to consider is myofibre water content which is known to decrease during growth [41] thus affecting water mobility.

Time dependence of ADC in both GA and TA muscles shows similar behaviour for *in vivo* (Figure 2) and *in vitro* (Figure 4) samples, which, illustrates the reproducibility of these data across animals and ages either *in vivo* or *in vitro*. Moreover, the comparison of ADC curves in TA and GA muscles, both *in vivo* (Figure 3) and *in vitro* (Figure 5) clearly show higher diffusivity for each age group in the TA muscle when measured parallel to myofibres and lower when measured transverse to fibres in keeping with known anisotropy of muscle fibres (16,20). We acknowledge that the myofibre main axis and the diffusion gradient direction may not be identical as our measurements were not made using a DTI sequence which would have required much longer acquisition times. Diffusion gradients were applied parallel and transverse to the tibial bone and therefore, measurements transverse or parallel to an axis were considered representative of muscle fibre direction. Measurements are likely to be better aligned with the TA than the GA muscle, but the bias is consistent between samples in all cases. The alignment of the applied diffusion-gradient

and GA muscle axis is the same across animals and this is reflected in the reproducibility of the data across animals and samples.

Conclusions

In vivo and *in vitro* ADC time-dependent measurements in young and mature muscles showed a decrease in water diffusivity with increasing mouse age. This is evidence of microstructural differences between young and adult muscles. Histological analysis of muscle tissue showed smaller fibre diameter in young mouse muscle, which increased with age, a feature that is counter to the observation of lower ADC in older muscle if the main determinant of tissue diffusivity is assumed to be muscle fibre membrane spacing. Further measures of extracellular space showed that these values were small and only differed by ~1% between ages. This strongly suggests that the influence of extracellular space on muscle ADC is likely to be negligible. We therefore suggest that the observed differences in ADC with age are best explained in terms of changes of membrane permeability.

Acknowledgments

We gratefully acknowledge Professor Miranda D Ground for helpful discussion.

This project has received funding from the European Union's Seventh Framework Programme for research, technological development and demonstration under grant agreement no 602485 (BIOIMAGE-NMD).

5. References

1. Janssen I, Heymsfield SB, Wang ZM, Ross R. Skeletal muscle mass and distribution in 468 men and women aged 18-88 yr. *J Appl Physiol.* 2000;89(1):81-8.
2. Sartori R, Schirwis E, Blaauw B, et al. BMP signaling controls muscle mass. *Nat Genet.* 2013;45(11):1309-18.
3. Clark KA, McElhinny ES, Beckerle MC, Gregorio CC. Striated muscle cytoarchitecture: an intricate web of form and function. *Annu Rev Cell Dev Biol.* 2002;18:637-706.
4. Schiaffino S, Dyar KA , Ciciliot S , Blaauw B, Sandri M. Mechanisms regulating skeletal muscle growth and atrophy. *FEBS J.* 2013;280(17):4294-314.
5. Sandri M. Signaling in muscle atrophy and hypertrophy. *Phyisology*. 2008; 23:160-70.
6. Grounds MD, Shavlakadze T. Growing muscle has different sarcolemmal properties from adult muscle: a proposal with scientific and clinical implications: reasons to reassess skeletal muscle molecular dynamics, cellular responses and suitability of experimental models of muscle disorders. *Bioessays.* 2011;33(6):458-68.
7. White RB, Bierinx A-S, Gnocchi VF, Zammit PS. Dynamics of muscle fibre growth during postnatal mouse development. *BMC Dev Biol.* 2010;10:21.
8. Butchart LC, Fox A, Shavlakadze T, Grounds MD. The long and short of non-coding RNAs during post-natal growth and differentiation of skeletal muscles: Focus on lncRNA and miRNAs. *Differentation*. 2016; 92(5):237-248.
9. Emery AEH. The muscular dystrophies. *The Lancet.* 2002;359(9307):687–95.
10. Bushby K, Finkel R, Birnkrant DJ, et al. Diagnosis and management of Duchenne muscular dystrophy, part 1: diagnosis, and pharmacological and psychosocial management. *The Lancet Neurol.* 2010;9(1):77-93.
11. Diffusion MRI: Theory, Methods, and Applications, vol1, Jones DK (ed). Oxford: Oxford University Press 2010.
12. Basser PJ. Inferring microstructural features and the physiological state of tissues from diffusion-weighted images. NMR Biomed. 1995; 8(7-8): 333-344.

13. Bammer R. Basic principles of diffusion-weighted imaging. *Eur J Radiol*. 2003;45(3):169-84.

14. Yablonskiy DA, Sukstanskii AL. Theoretical models of the diffusion weighted MR signal. *NMR Biomed.* 2010; 23(7): 661-681.

15. Karampinos DC, King KF, Sutton BP, Georgiadis JG. In vivo study of cross-sectional skeletal muscle fiber asymmetry with diffusion-weighted MRI. *Conf Proc IEEE Eng Med Biol Soc*. 2007;2007:327-30.

16. Heemskerk AM, Damon BM. Diffusion tensor MRI assessment of skeletal muscle architecture. *Curr Med Imaging Rev*. 2007;3:152–160.

17. Strijkers GJ, Drost MR, Nicolay K. Diffusion Imaging in muscle. In: Jones DK ed. Diffusion MRI: Theory, Methods, and Applications, vol 1 Oxford: Oxford University Press 2010:672-683.

18. Schwenzer NF, Steidle G, Martirosian P, Schraml C, Springer F, Claussen CD, Schick F. Diffusion tensor imaging of the human calf muscle: distinct changes in fractional anisotropy and mean diffusion due to passive muscle shortening and stretching. *NMR Biomed*. 2009 Dec;22(10):1047-53.

19. Mazzoli V, Oudeman J, Nicolay K, Maas M, Verdonschot N, Sprengers AM, Nederveen AJ, Froeling M, Strijkers GJ. Assessment of passive muscle elongation using Diffusion Tensor MRI: Correlation between fiber length and diffusion coefficients. *NMR Biomed*. 2016;29(12):1813-1824.

20. Damon BM, Froeling M, Buck AK, Oudeman J, Ding Z, Nederveen AJ, Bush EC, Strijkers GJ. Skeletal muscle diffusion tensor-MRI fiber tracking: rationale, data acquisition and analysis methods, applications and future directions. *NMR Biomed*. 2017;30(3) DOI: 10.1002/nbm.3563.

21. Briguet A, Curdier-Fruh I, Foster M, Meier T, Magyar JP. Histological parameters for the quantitative assessment of muscular dystrophy in the mdx-mouse. *Neuromusc Disord.* 2004; 14(10):675-82

22. Tanner JE. Self diffusion of water in frog muscle. *Biophys J.* 1979; 28(1): 107-116

23. Fieremans E, Lemberskiy G, Veraart J, Sigmund EE, Gyftopoulos S, Novikov DS. *In vivo* measurement of membrane permeability and myofiber size in human muscle using time-dependent diffusion tensor imaging and the random permeable barrier model. *NMR Biomed.* 2017; 30(3) DOI: 10.1002/nbm.3612.

24. Kim S, Chi-Fishman G, Barnett AS, Pierpaoli C. Dependence on diffusion time of apparent diffusion tensor of ex vivo calf tongue and heart. *Magn Reson Med*. 2005;54(6):1387-96.

25. Steidle G, Schick F. Echoplanar diffusion tensor imaging of the lower leg musculature using eddy current nulled stimulated echo preparation. *Magn Reson Med*. 2006;55(3):541-8.

26. Sigmund EE, Novikov DS, Sui D et al. Time-dependent diffusion in skeletal muscle with the random permeable barrier model (RPBM): application to normal controls and chronic exertional compartment syndrome patients. *NMR Biomed*. 2014;27(5):519-28.

27. Marschar AM, Kuder TA, Stieltjes B, Nagel AM, Bachert P, Laun FB. In vivo imaging of the time-dependent apparent diffusional kurtosis in the human calf muscle. *J Magn Reson Imaging*. 2015;41(6):1581-90.

28. De Santis S, Jones DK, Roebroeck A. Including diffusion time dependence in the extra-axonal space improves in vivo estimates of axonal diameter and density in human white matter. *Neuroimage*. 2016;130:91-103.

29. Fieremans E, Burcaw LM, Lee HH, Lemberskiy G, Veraart J, Novikov DS. In vivo observation and biophysical interpretation of time-dependent diffusion in human white matter. *Neuroimage*. 2016 Apr 1;129:414-27.

30. Zhou IY, Gao DS, Chow AM, Fan S, Cheung MM, Ling C, Liu X, Cao P, Guo H, Man K, Wu EX. Effect of diffusion time on liver DWI: an experimental study of normal and fibrotic livers. *Magn Reson Med*. 2014;72(5):1389-96.

31. Lemberskiy G, Rosenkrantz AB, Veraart J, Taneja SS, Novikov DS, Fieremans E. Time-Dependent Diffusion in Prostate Cancer. *Invest Radiol*. 2017; 52(7):405-411.

32. Porcari P, Hegi ME, Lei H, Hamou MF, Vassallo I, Capuani S, Gruetter R, Mlynarik V. Early detection of human glioma sphere xenografts in mouse brain using diffusion MRI at 14.1 T. *NMR Biomed*. 2016 ;29(11):1577-1589.

33. Novikov DS, Fieremans E, Jensen JH, Helpern JA. Random walks with barriers. *Nat Phys.* 2011;7(6):508–514.

34. Tanner J. Use of the stimulated echo in NMR diffusion studies. *J Chem Phys.* 1070;52(5):2523.

35. Stejskal EO, Tanner E. Spin diffusion measurements: spin echoes in the presence of a time-dependent field gradient. *J Chem Phys.* 1967;42(1):288-292.

36. Clark CA, Hedehus M, Moseley ME. Diffusion time dependence of the apparent diffusion tensor in healthy human brain and white matter disease. *Magn Reson Med*. 2001; 45:1126-1129.

37. Hall MG, Clark CA. Diffusion in hierarchical systems: A simulation study in models of healthy and diseased muscle tissue. *Magn Reson Med.* 2016 25. doi: 10.1002/mrm.26469.

38. Clark CA, Le Bihan D. Water diffusion compartmentalization and anisotropy at high b values in human brain. *Magn Reson Med*. 2000; 44:852:859.

39. Sakellariou GK, Pearson T, Lightfoot AP, Nye GA, Wells N, Giakoumaki II, Vasilaki A, Griffiths RD, Jackson MJ, McArdle A. Mitochondrial ROS regulate oxidative damage and mitophagy but not age-related muscle fiber atrophy. *Sci Rep.* 2016;29:6:33944. doi:10.1038/srep33944.

40. Straub V, Rafael GA, Chamberlain JS, Campbell KP. Animal Models for Muscular Dystrophy Show Different Patterns of Sarcolemmal Disruption. *J Cell Biol.* 1997; 139(2): 375–38.

41. The Structure and Function of Muscle vol 1, Bourne GH (ed.). New York: Academic Press; 1972.

Table1. DWI protocol. Summary of *b*-values used in the DWI acquisitions for each diffusion time (Δ).

	b-values [s/mm^2]					
	Δ=25ms	Δ=60ms	Δ=100ms	Δ=150ms	Δ=250ms	Δ=350ms
b_0	14	44	78	121	208	294
b_1	550	550	550	550	550	550
b_2	-	1100	1100	1100	1100	1100

A missing value (-) indicates no *b*-value available.
The calculation of *b*-values includes the contribution of imaging and crusher gradients leading to non-zero b_0 values for the un-weighted diffusion images.

Table 2. Summary of *in vivo* ADC values calculated in the gastrocnemius (GA) and tibialis anterior (TA) muscles of wild type mice of three age groups (7.5-, 22- and 44-week-old).

Δ [ms]	ADC [10^{-3} mm^2/s]											
	Gastrocnemius (GA) muscle						Tibialis anterior (TA) muscle					
	Gdiff transverse to fibres			Gdiff parallel to fibres			Gdiff transverse to fibres			Gdiff parallel to fibres		
	7.5 weeks	22 weeks	44 weeks	7.5 weeks	22 weeks	44 weeks	7.5 weeks	22 weeks	44 weeks	7.5 weeks	22 weeks	44 weeks
25	1.13 ± 0.03¶	0.99 ± 0.02	0.97 ± 0.03	1.68 ± 0.05¶	1.49 ± 0.02#	1.52 ± 0.04#	1.10 ± 0.03	1.02 ± 0.02	0.98 ± 0.03	1.80 ± 0.03¶	1.59 ± 0.03	1.59 ± 0.03
60	0.99 ± 0.03¶¥	0.83 ± 0.02	0.82 ± 0.04	1.50 ± 0.04	1.32 ± 0.02#	1.35 ± 0.02	0.94 ± 0.02	0.84 ± 0.02	0.82 ± 0.02	1.63 ± 0.03¶	1.44 ± 0.03	1.45 ± 0.04
100	0.89 ± 0.02¶¥	0.74 ± 0.02	0.69 ± 0.02	1.48 ± 0.04	1.31 ± 0.02#	1.29 ± 0.03	0.88 ± 0.02¶¥	0.70 ± 0.01	0.68 ± 0.02	1.60 ± 0.03¶¥	1.41 ± 0.02	1.42 ± 0.01
150	-	0.66 ± 0.02	0.64 ± 0.02	-	1.28 ± 0.02	1.27 ± 0.02	-	0.60 ± 0.01	0.63 ± 0.02	-	1.39 ± 0.02	1.37 ± 0.04
250	0.69 ± 0.02	0.61 ± 0.02#	0.57 ± 0.02	1.43 ± 0.03¶¥	1.25 ± 0.02#	1.24 ± 0.02	0.67 ± 0.01¶¥	0.53 ± 0.01	0.53 ± 0.01	1.52 ± 0.02¶¥	1.35 ± 0.02	1.33 ± 0.02
350	0.65 ± 0.02	0.58 ± 0.01#	0.54 ± 0.05	1.35 ± 0.02¶¥	1.19 ± 0.01#	1.18 ± 0.02	0.62 ± 0.01¶¥	0.48 ± 0.01	0.48 ± 0.01	1.39 ± 0.02¶¥	1.27 ± 0.01	1.26 ± 0.02

ADC values were obtained by applying the diffusion gradient (Gdiff) parallel or transverse to muscle fibres. Data are mean ± 1 s.e.m.
A missing value (-) indicates no DW images available for the evaluation of the ADC.
Statistics: ¶ significantly different from the corresponding ADC value calculated by applying the diffusion gradient along the same direction in mice aged 22 weeks (one-way ANOVA followed by Tuckey post-hoc test, $p < 0.01$); ¥ significantly different from the corresponding value calculated by applying the diffusion gradient along the same direction in mice aged 44 weeks (one-way ANOVA followed by Tuckey post-hoc test, $p < 0.01$); # significantly different from the corresponding value in the TA muscle (paired two-tailed t test, $p < 0.05$).

Table 3. Summary of in vivo T_1 relaxation times measured in the gastrocnemius (GA) and tibialis anterior (TA) muscles from wild-type mice of three age groups (7.5-, 22- and 44-week-old). Data are mean ± 1 s.e.m.

muscle	T_1 [ms]		
	7.5 weeks	22 weeks	44 weeks
GA	827 ± 22	843 ± 29	856 ± 23
TA	826 ± 21	840 ± 13	838 ± 22

Statistics: ¶ significantly different from the corresponding T_1 calculated in mice aged 22 weeks (one-way ANOVA followed by Tuckey post-hoc test, $p < 0.01$); ¥ significantly different from the corresponding T_1 calculated in mice aged 44 weeks (one-way ANOVA followed by Tuckey post-hoc test, $p < 0.01$); #significantly different from the corresponding value in the TA muscle (paired two-tailed t test, $p < 0.05$).

Table 4. Summary of *in vitro* ADC values calculated in the gastrocnemius (GA) and tibialis anterior (TA) muscles from excised hind-limbs of wild type mice of three age groups (7.5-, 22- and 44-week-old).

Δ [ms]	ADC [10^{-3} mm^2/s]											
	Gastrocnemius (GA) muscle						Tibialis anterior (TA) muscle					
	Gdiff transverse to fibres			Gdiff parallel to fibres			Gdiff transverse to fibres			Gdiff parallel to fibres		
	7.5 weeks	22 weeks	44 weeks	7.5 weeks	22 weeks	44 weeks	7.5 weeks	22 weeks	44 weeks	7.5 weeks	22 weeks	44 weeks
25	0.75 ± 0.01	0.75 ± 0.01	0.73 ± 0.02	0.99 ± 0.01¶¥	0.882 ± 0.005#	0.92 ± 0.02	0.70 ± 0.02	0.73 ± 0.02	0.74 ± 0.02	0.95 ± 0.02	0.92 ± 0.01	0.93 ± 0.01
60	0.67 ± 0.01¥	0.631 ± 0.009	0.62 ± 0.02	0.90 ± 0.01¶¥	0.797 ± 0.004	0.80 ± 0.01	0.66 ± 0.02	0.63 ± 0.01	0.63 ± 0.02	0.92 ± 0.02¶	0.84 ± 0.02	0.83 ± 0.01
100	0.62 ± 0.01	0.564 ± 0.005	0.57 ± 0.02	0.86 ± 0.01¶¥#	0.748 ± 0.003#	0.761 ± 0.007	0.61 ± 0.01	0.572 ± 0.009	0.58 ± 0.01	0.90 ± 0.01¶¥	0.80 ± 0.01	0.79 ± 0.01
150	-	0.530 ± 0.004	0.52 ± 0.01	-	0.730 ± 0.003#	0.736 ± 0.006	-	0.537 ± 0.009	0.54 ± 0.01	-	0.783 ± 0.008	0.77 ± 0.01
250	0.56 ± 0.01¶¥	0.492 ± 0.005	0.49 ± 0.01	0.82 ± 0.01¶¥#	0.705 ± 0.003#	0.71 ± 0.01	0.57 ± 0.02¶	0.505 ± 0.009	0.51 ± 0.01	0.89 ± 0.02¶¥	0.757 ± 0.009	0.73 ± 0.01
350	0.55 ± 0.01¶¥	0.477 ± 0.005	0.47 ± 0.02#	0.80 ± 0.01¶¥#	0.685 ± 0.003#	0.69 ± 0.01	0.56 ± 0.02¶	0.50 ± 0.01	0.51 ± 0.01	0.88 ± 0.02¶¥	0.742 ± 0.008	0.73 ± 0.01

ADC values were obtained by applying the diffusion gradient (Gdiff) parallel or transverse to muscle fibres. Data are mean ± 1 s.e.m.
A missing value (-) indicates no DW images available for the evaluation of the ADC.
Statistics: ¶ significantly different from the corresponding ADC value calculated in mice aged 22 weeks with the diffusion gradient applied along the same direction (one-way ANOVA followed by Tuckey post-hoc test, $p < 0.01$); ¥ significantly different from the corresponding ADC value calculated in mice aged 44 weeks with the diffusion gradient applied along the same direction (one-way ANOVA followed by Tuckey post-hoc test, $p < 0.01$); # significantly different from the corresponding value in the TA muscle (paired two-tailed t test, $p < 0.05$).

Table 5. Comparison between the percentages of Evans Blue Dye (EBD) uptake in the gastrocnemious (GA) and tibialis anterior (TA) muscles from wild-type mice of three age groups.

muscle	P (*percentage of EBD+ area*)		
	7.5 weeks	22 weeks	44 weeks
GA	2.7 ± 0.5	1.5 ± 0.1	1.3 ± 0.4
TA	0.78 ± 0.02	0.57 ± 0.01	0.31 ± 0.02

Figure Captions

Figure 1. *In vivo* MRI of hind-limb muscles from a mouse aged 7.5 weeks.

Left panel: T_2-w image of a mouse hind-limb (A) acquired with axial orientation to the tibial bone. Regions-of-interest (ROIs) drawn as circular areas (0.026 mm^2) in the tibialis anterior (TA) muscle (ROI 1, red) and the gastrocnemius (GA) muscle (ROI 2, green) are shown. Right upper panel: representative diffusion-weighted image (B) and corresponding ADC map (C) of muscle hind-limb acquired with the diffusion gradient (Gdiff) parallel to fibres, diffusion time (Δ) and *b*-value equal to 250 ms and 550 s/mm^2, respectively. Right lower panel: representative diffusion-weighted image (D) and corresponding ADC map acquired with Gdiff transverse to fibres, Δ = 250 ms and *b*-value = 550 s/mm^2.

Figure 2. *In vivo* hind-limb muscle mean ADC values as a function of diffusion time (Δ).

Mean ADC values of the gastrocnemius (GA) muscle (A) and tibialis anterior (TA) muscle (B) were measured from mice aged 7.5 (black lines), 22 (green lines) and 44 (red lines) weeks of age by applying the diffusion gradient (Gdiff) parallel (dashed lines) or transverse (solid lines) to muscle fibres. For each Δ, ADC of each muscle per mouse and age group were determined by fitting the corresponding DWI data with a mono-exponential equation. Accuracy of each individual fit was $r^2 \leq 0.99$.

Figure 3. Comparison between *in vivo* mean ADC values of the gastrocnemius (GA) and the tibialis anterior (TA) muscles as function of Δ.

Mean ADC values of the GA (filled symbols) and the TA (open symbols) muscles from mice aged 7.5 (plot A, black lines), 22 (plot B, green lines) and 44 weeks (plot C, red lines) were measured by applying the diffusion gradient (Gdiff) transverse (solid lines) or parallel (dashed lines) to muscle fibres. The vertical axes of both graphs B and C have the same scale and units as graph A. For each Δ, ADC of each muscle per mouse and age group were determined by fitting the corresponding DWI data with a mono-exponential equation. Accuracy of each individual fit was $r^2 \leq 0.99$.

Figure 4. *In vitro* hind-limb muscle mean ADC values as function of diffusion times (Δ).

Mean ADC values of the gastrocnemius (GA) muscle (A) and the tibialis anterior (TA) muscle (B) were measured in hind-limbs fixed in formalin for 24 hours from mice aged 7.5 (black lines), 22 (green lines) and 44 (red lines) weeks. In both muscles, ADC values were measured by applying the diffusion gradient (Gdiff) parallel (dashed lines) or transverse (solid lines) to muscle fibres, as for *in vivo* measurements. For each Δ, ADC of each muscle per mouse and age group were determined by fitting the corresponding DWI data with a mono-exponential equation. Accuracy of each individual fit was $r^2 \leq 0.99$.

Figure 5. Comparison between *in vitro* mean ADC values of the gastrocnemius (GA) and the tibialis anterior (TA) muscles as a function of Δ.

Mean ADC values of the GA (filled symbols) and the TA (open symbols) muscles were measured in hind-limbs fixed in formalin and excised from mice aged 7.5 (plot A, black lines), 22 (plot B, green lines) and 44 weeks (plot C, red lines). In both muscles, ADC values were measured by applying the diffusion gradient (Gdiff) parallel (dashed lines) or transverse (solid lines) to muscle fibres, as for *in vivo* measurements. For each Δ, ADC of each muscle per mouse and age group were determined by fitting the corresponding DWI data with a mono-exponential equation. Accuracy of each individual fit was $r^2 \leq 0.99$.

Figure 6. H&E staining and histological analysis.

Upper panel: selected areas from H&E stained medial cross-section of the gastrocnemius (GA) muscle, dissected from mice aged 7.5 (A), 22 (B) and 44 (C) weeks, respectively. Images A, B and C, displayed with the same magnification (scale bar 100 μm), show differences in muscle fibre size according to age. Middle panel: frequency histograms of muscle fibre size of GA (D) and TA muscles (E) for mice aged 7.5 (black), 22 (green) and 44 (red) weeks. Lower panel: comparison between GA (filled symbols) and TA (open symbols) frequency histograms of muscle fibre size for mice aged 7.5 (F) (black), 22 (G) (green) and 44 (H) (red) weeks, respectively.

Figure 7. Comparison between the percentage, *P*, of Evans Blue Dye (EBD) uptake determined from the gastrocnemius (GA) (filled symbols) and the tibialis anterior (TA) (open symbols)

muscles of wild-type mice aged 7.5 (black), 22 (green) and 44 (red) weeks. Histological section of the GA muscle showing the EBD positive uptake in healthy mice is also displayed.

Figure 1

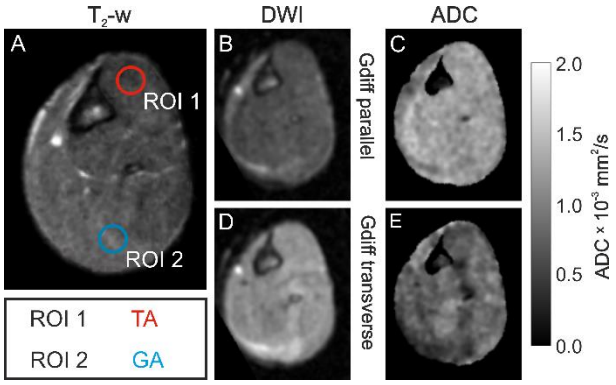

Figure 2

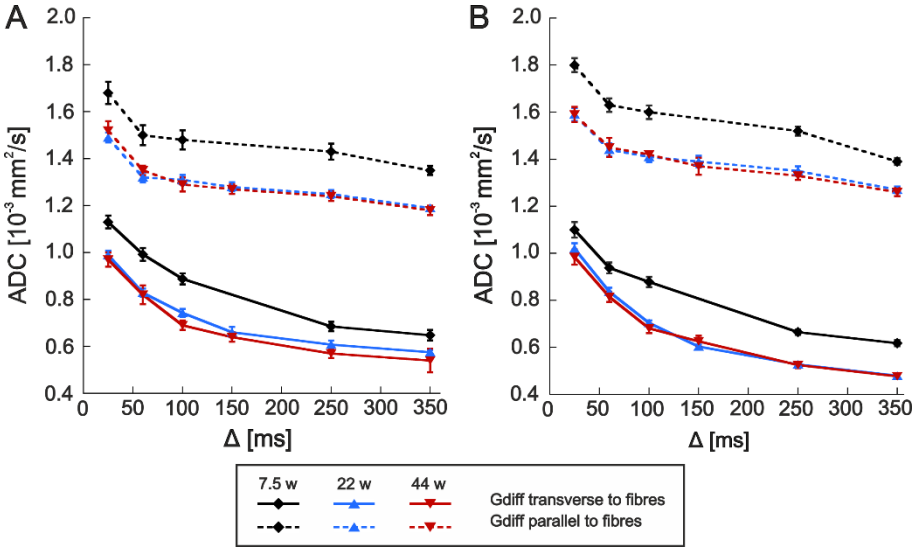

Figure 3

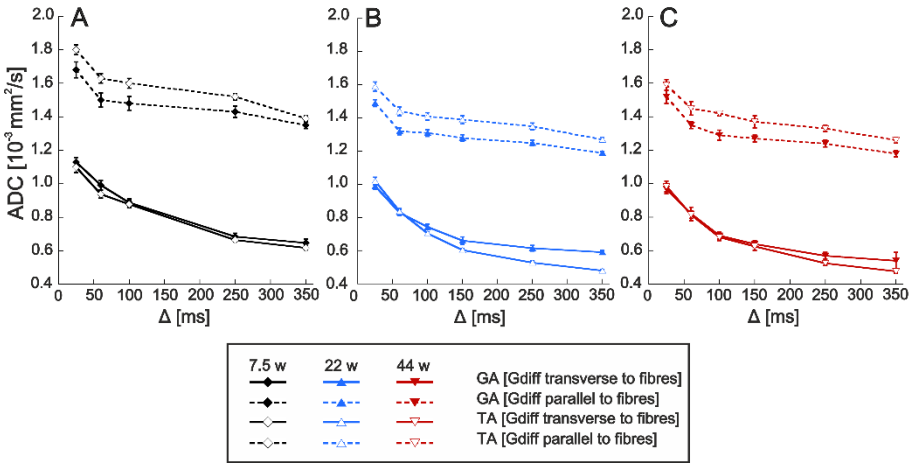

Figure 4

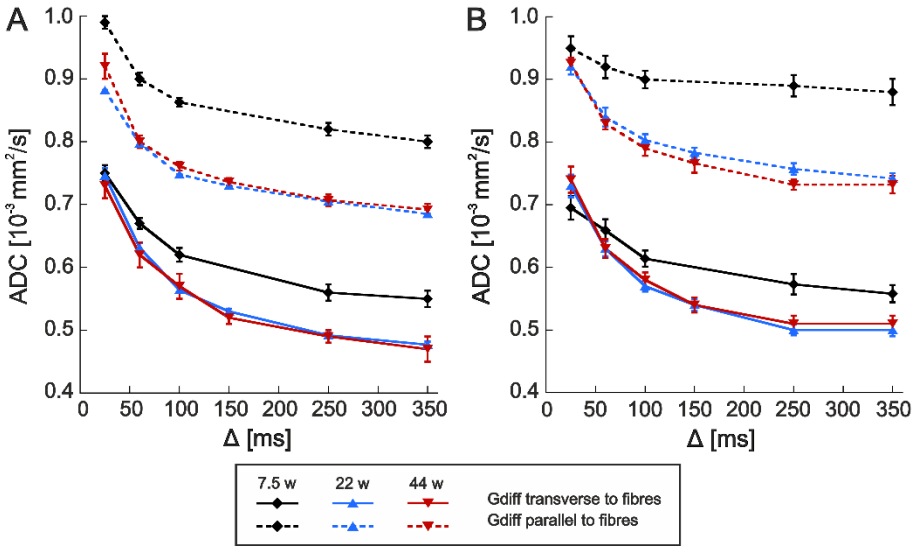

Figure 5

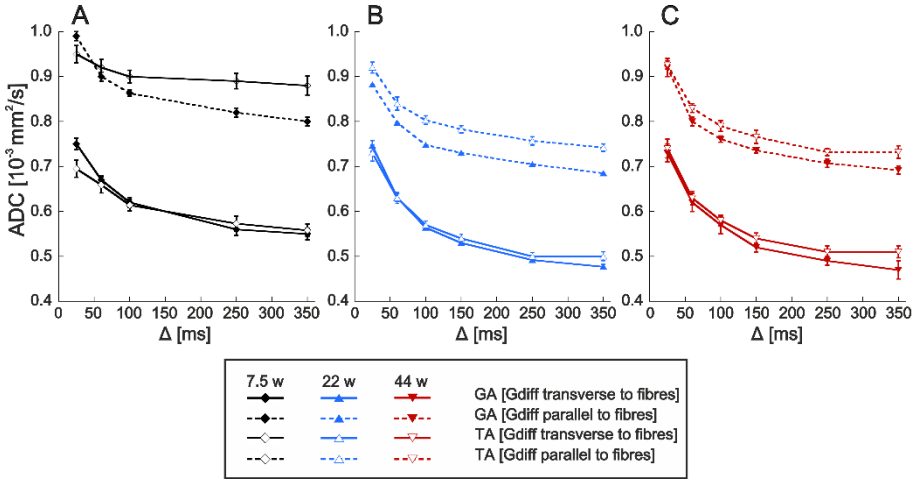

Figure 6

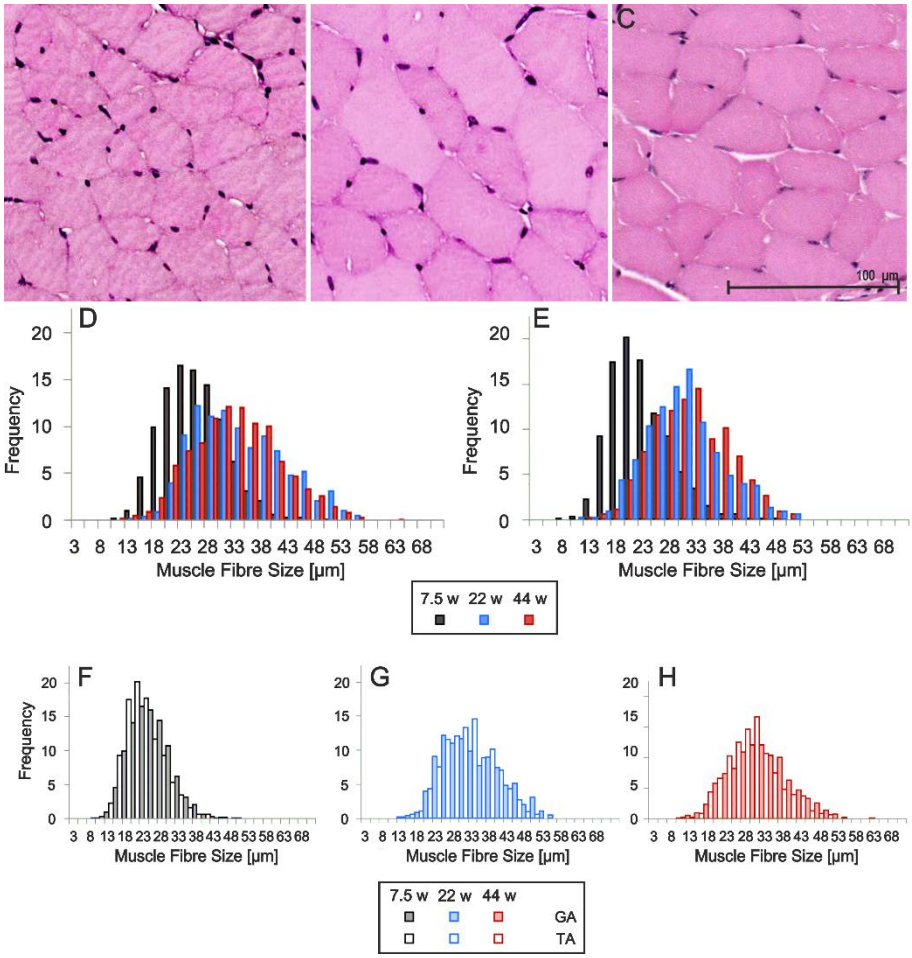

Figure 7